Molecular Dynamics Simulation of Nanostructural Organization in Ionic Liquid/Water Mixtures†

Wei Jiang, Yanting Wang, and Gregory A. Voth*

Center for Biophysical Modeling and Simulation and Department of Chemistry, University of Utah, Salt Lake City, Utah 84112-0850

Received: October 30, 2006; In Final Form: January 4, 2007

Molecular dynamics simulations have been carried out to investigate nanostructural organization in mixtures of 1-octyl-3-methylimidazolium nitrate ionic liquid and water at multiple water concentrations. Evolution of the polar network, water network, and micelle structures is visualized and analyzed via partial radial distribution functions. The calculated static partial structure factors show that within the range of water contents examined, polar networks, water networks, and micelles possess an approximately invariant characteristic length at around 20 Å. Furthermore, the above calculations point out that, as the amount of water increases, the polar network is continuously broken up (screened) by the intruding water, while the structural organization of the water network and the micelle exhibits a *turnover*. At the turnover point, the most ordered micelle (cation−cation) structure and water (water−anion−water) network are formed. Thereafter, the structural organization abates drastically, and only loose micelle structure exists due to the dominant water−water interactions. The simulated turnover of structural organization agrees with the sharpest peak in the experimentally obtained structure factor in aqueous solutions of similar ionic liquids; the simulated water structure reveals that water can form liquidlike associated aggregates due to the planar symmetry and strong basicity of NO_3^-, in agreement with experiment. The turnover of structural organization of micelles results from the persistent competition between the hydrophobic interactions of the nonpolar groups and the breakup of the charged polar network with increasing water content, whereas the turnover of the water network results from the competition between the water−water and water−anion interactions.

I. Introduction

Room temperature ionic liquids (RTILs) have received considerable attention due to their potential as an environmentally friendly alternative to traditional organic solvents.[1−3] RTILs exhibit many desirable properties, such as vanishing vapor pressure, broad thermal stability, high polarity, characteristic electrical conductivity, the ability to dissolve a range of inorganic solvents, etc. The collection of these properties has also motivated their use in catalysis and organic/inorganic synthesis.[4−6]

In recent years, the imidazolium-based ionic liquids (ILs) have attracted considerable interest. Specifically, the structure of these IL systems exhibits unique spatial heterogeneity that results from their inherent polar/nonpolar phase separation. Both experiments and computational work have shown that these ILs, with a moderate or long alkyl tail, show a prominent microphase segregation structure both in the bulk and at the interface. Seddon and co-workers[4,6] and Lee and co-workers[7,8] reported experimental work in which a liquid crystal phase was observed for pure ILs with long alkyl tails. Hamaguchi and Ozawa[9] performed Raman spectroscopic and X-ray diffraction studies of 1-butyl imidazolium-based ILs and revealed that ILs may form a mesophase that is distinct from the liquid crystal phase due to the local structure formation near the butyl group. Urahata and Ribeiro[10] reported the occurrence of an intermediate range order in the presence of long alkyl tails. Margulis[11] calculated the distribution of the cavities in these ILs and found the existence of long-lived cavities for long-chained ILs. More recently,[12−14] a nanostructural organization in pure 1-alkly-3-methylimidazolium based ILs with various alkyl chain lengths was shown computationally. In these latter studies, two distinct domains are formed: The charged imidazolium rings and anions form a 3-D polar network due to their strong electrostatic interaction, while the charge-neutral nonpolar groups aggregate and form a nonpolar domain controlled by the short-range Van der Waals interactions. Both experimental[15,16] and computational[17−21] work suggests that similar phase separation exists at the IL/vacuum interface, where the nonpolar groups point out to the gas phase while the polar groups are directed more deeply into the bulk.

The significance of the interaction between water and RTILs has been well-recognized, given the fact that the ILs are hygroscopic and can absorb a significant amount of water from the atmosphere.[22−26] Seddon et al.[27] reported a systematic study of the effect of impurities and additives, for example, water, chloride, and cosolvents, on the physical properties of imidazolium-based ionic liquids, and it was discovered that the viscosity and density not only are changed by the presence of water but also strongly depend on the molar fraction of the water added. With attenuated total reflectance and transmission infrared spectroscopy, Cammsrata et al.[26] have systematically investigated the physical state of water in RTILs. They showed that water is mostly present in two states, depending on the strength of basicity of anion. In Rivera-Rubero and Baldelli's work,[28] the different influence of water on the surface of

† Part of the special issue "Physical Chemistry of Ionic Liquids".

* To whom correspondence should be addressed. E-mail: voth@chem.utah.edu.

10.1021/jp067142l CCC: $37.00
Published on Web 02/27/2007

hydrophobic and hydrophilic ILs was reported. Saha and Hamaguchi[29] employed single-crystal X-ray crystallography and near-infrared Raman spectroscopy to investigate the water effect on IL structure; distinct molecular structures and arrangements of ILs with and without water were observed. Hanke and Lynden-Bell[30] performed a molecular dynamics (MD) simulation of mixtures of 1,3-dialkyl imidazolium ionic liquids and water to investigate the microscopic physical properties as a function of composition. They provided the first molecular-level picture for the water structure in an IL/water mixture, and the water-enhanced ion dynamics was investigated, as well. More recently, Lopes et al.[31] performed a structural analysis on the solvation of nonpolar, polar, and associating solutes in imidazolium-based ionic liquids, and they showed that the existence of microphase segregation between polar and nonpolar domains in ionic liquids changes the way in which solvation can be understood.

The influence of water on the nanostructural organization of ILs has been a central focus due to its potential application to synthetic chemistry and catalysis. By studying water-induced acceleration of ion diffusion, Dupont et al.[32] proposed that imidazolium-based ILs have polar and nonpolar regions, especially when a controlled amount of water is added. Therefore, ILs may be regarded as nanostructured materials.[33] Bowers et al.[34] systematically investigated the aggregation behavior in aqueous solutions of three ionic liquids on the basis of the 1-alkyl-3-methylimidazolium cation by means of surface tension, conductivity, and small angle neutron scattering (SANS) measurements, which probed the sizes and shapes of the aggregates. In the work of Firestone et al.,[35] the addition of water to 1-decyl-3-methylimidazolium bromide was shown to result in its spontaneous self-organization and the concomitant formation of a liquid-crystalline gel, thus providing a potentially simple means of preparing a supramolecular assembly comprising a RTIL. Antonietti et al.[36] showed that with water applied to IL, the IL plays the role of a classical surfactant having a very strong tendency toward self-organization with high order. Turmine et al.[37] confirmed the existence of a surface transition for aqueous solutions of imidazolium-based ionic liquids and indicated that the transition probably corresponds to the aggregation of electrolytes.

Despite the numerous computational and experimental studies on water/IL mixtures, to date, our knowledge of the interaction between water and ILs remains somewhat empirical. In the present study, the focus will be on the effects of varying water concentrations on the nanostructural organization of a particular IL, 1-octyl-3-methylimidazolium nitrate ($OMIM^+/NO_3^-$). Our intent is to achieve a more detailed molecular-level understanding of the underlying mechanisms of the nanostructural organization. In our previous work, it was found that dry $OMIM^+/NO_3^-$ shows prominent phase separation both in bulk and at the vacuum/IL interface.[13,21] MD simulations of IL/water mixtures at various water contents are reported here, with a detailed discussion of the breakup of the polar domain, water-accelerated ion diffusion, the formation of a water−anion−water network, and the nonpolar group aggregation.

The remainder of this paper is organized as follows: In Section II, the atomistic models and simulation methodology are described. Section III reports the MD simulation results, and a discussion is given. Section IV then provides concluding remarks.

II. Models and Simulation Methodology

A. Atomistic Force Field. The total potential energy function was described by a sum of bond, angle, dihedral deformation energies, van der Waals (in the Lennard-Jones (LJ) 6−12 form), and Coulombic interactions. Such force fields are of a standard form, given by

$$V = \sum_{\text{bonds}} k_b(r - r_0)^2 + \sum_{\text{angle}} k_\theta(\theta - \theta_0)^2 + \sum_{\text{dihedrals}} V_n \cos(n\phi - \gamma) + \sum_i \sum_{j>i} \left(\frac{a_{ij}}{r_{ij}^{12}} - \frac{b_{ij}}{r_{ij}^{6}} + \frac{q_i q_j}{r_{ij}} \right) \quad (1)$$

In the above equation, the force field parameters for the IL are provided in the standard Amber force field[38] and have been used in previous work.[20,39,40] The partial charges of both cations and anions were obtained by fitting the ab initio electrostatic potentials (ESP) with the RESP fitting package.[13] The ab initio calculations were performed with Gaussian 03.[41] The ESP grids were generated by MP2/6-31G(d) and fit to the MP2/6-31G(d) optimized structure. For the water, the SPC/Fw water model along with the force field parameters developed by Wu et al.[42] were employed. For unlike atoms, the LJ parameters are obtained from the Lorentz−Berthelot (LB) combining rules. Note that the electronically nonpolarizable version of the force field was used in this work, since it is faster in the MD execution, and the qualitative features of the IL/water systems were the target of these studies.

TABLE 1: Sizes for Different Simulated Systems

molar fraction of water, %	ion pairs	no. water molecules	aimulation cell size (X, Y, Z), Å
0	512	0	59.3, 59.3, 59.3
20	512	128	59.6, 59.6, 59.6
50	512	512	60.4, 60.4, 60.4
66.7	512	1024	61.6, 61.6, 61.6
75	512	1536	62.7, 62.7, 62.7
80	512	2048	64.0, 64.0, 64.0
90.9	64	640	35.5, 35.5, 35.5
95.2	64	1280	40.1, 40.1, 40.1

B. Molecular Dynamics Simulation Details. In the MD simulations, the mixtures investigated had a mole fraction of water of $w = 0$, 20, 50, 66.7, 75, 80, 90.91, and 95.2%; the numbers of ion pairs used in each system depended on the mixture and computational feasibility. The parameters for the various systems are given in Table 1.

For the systems with water mole fraction from 0 to 80%, an accelerated equilibration strategy was performed and consisted of five distinct steps: In step 1, an initial configuration containing 64 ion pairs and water molecules of the corresponding mole fraction was manually constructed, with the ions and water molecules positioned on selected lattice positions within a large cubic simulation box. The initial configuration was then equilibrated at $T = 400$ K with a constant NPT simulation for 1 ns. The final configuration at $T = 400$ K was then reequilibrated under constant NVT conditions for 1 ns. In step 2, the fully equilibrated configuration was duplicated once in each dimension to get an initial configuration with 512 ion pairs. In step 3, the new configurations were then equilibrated at $T = 400$ K with a constant NPT simulation for 1 ns. In step 4, the volume was set to be the average volume obtained from the constant NPT run, and the systems were then equilibrated in a constant NVT ensemble at 700 K. The final configuration of 700 K was then cooled down sequentially to 400 K, at intervals of 100 K. For 700, 600, and 500 K, the system was equilibrated for 200 ps each, but for 500 ps for 400 K, adding up to a total preequilibration run of 1.1 ns. In step 5, the preequilibrated configuration was run under constant NVT conditions for 1 ns as a production run, during which the

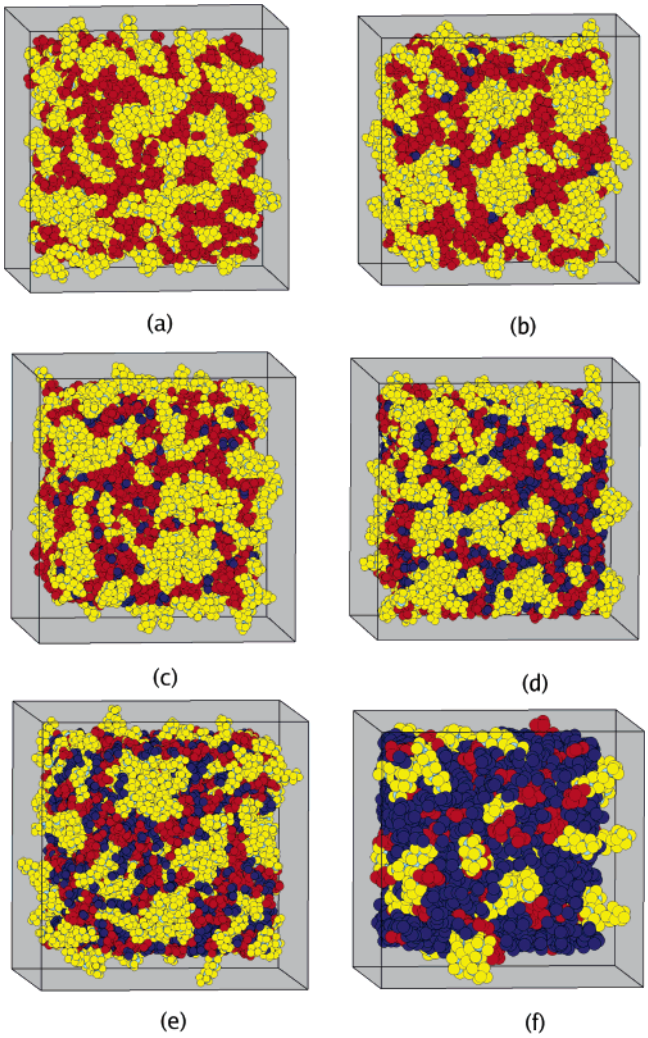

Figure 1. Snapshots of six selected simulation cells, taken from the MD trajectory data. The polar groups, nonpolar groups, and water are colored red, yellow, and dark blue, respectively. (a) Dry IL sample, (b) mixture with water of 20% mole fraction, (c) 50% mole fraction, (d) 75% mole fraction, (e) 80% mole fraction, (f) 95.2% mole fraction.

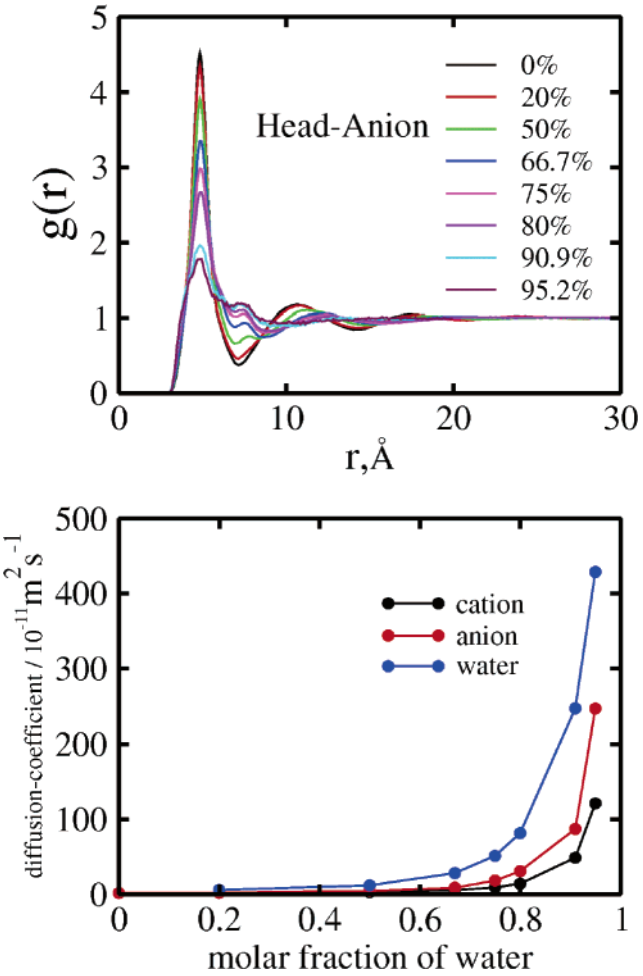

Figure 2. Breakup of the cation head−anion electrostatic network and enhanced diffusion with increasing water mole fraction. Upper panel, radial distribution functions of cation head group−anion (center of mass); lower panel, self-diffusion coefficients of the mixtures of various water concentrations, calculated by the general Einstein relation. Note that, corresponding to the trend of main peaks of radial distribution functions, the diffusion of water and ions are very slow until the water content is greater than 50% mole fraction. Thereafter, the diffusion increases considerably.

trajectory data was saved each 0.1 ps. The integration time step was 1.0 fs. For the mixtures with mole fraction of water at 90.91 or 95.2%, the same set of protocols was used, with the exception of the cell duplication in step 2. All simulations were carried out using the DL_POLY 2.13 package.[43] During the 400 K constant NPT run, no detectable vapor pressure was observed.

III. Results and Discussion

A. Visualization of Structures. All atom types were divided into three classes: polar, water, and nonpolar. In the forthcoming figures, these three types will be represented by three different colors. The NO_3^-, the aromatic ring of the cation, and the single methyl group bonded to the ring were designated the polar groups and shown as red. The whole alkyl chain was defined as the nonpolar group and colored yellow, and the water molecules are shown as dark blue. The term "head" is used to specifically refer to the imidazolium ring of the cation, and the term "tail" is used to refer to the terminal methyl group on the alkyl chain of the cation. The term "fraction + %" refers to the mole fraction of water in the mixture.

Figure 1 provides a general picture for the structure of the IL/water mixture with an increasing water content. All six panels are snapshots taken from the MD trajectory data during a production run. As a reference, panel a shows the phase separation of dry $OMIM^+/NO_3^-$, where clear nonpolar and polar phase separation can be observed. This picture is consistent with our former observations[12,13] and those of Lopes and Pàdua.[14] In panels b−e, it can be seen that the phase separation remains, with more and more water molecules embedded in the head−anion polar network. As the limiting case, panel f shows that the polar/nonpolar phase separation has been well-diluted by the water clusters, with the ions dispersed in the water clusters. Guided by this visual picture, a more systematic calculation of structure and dynamics was performed to obtain quantitative information, as described below.

B. Polar Network, Water Network, and Micelle Structure. Intuitively, it might be expected that the intruding water would break up the head−anion polar network so that the spatial correlation of head−anion monotonically decreases. This scenario proves to be the case. In Figure 2a, it can be seen that the height of the main peaks of head−anion radial distribution functions (RDFs) continuously decrease. Correspondingly, as illustrated in Figure 2b, the ion diffusion coefficients continuously increase, though they do so nonmonotonically with a

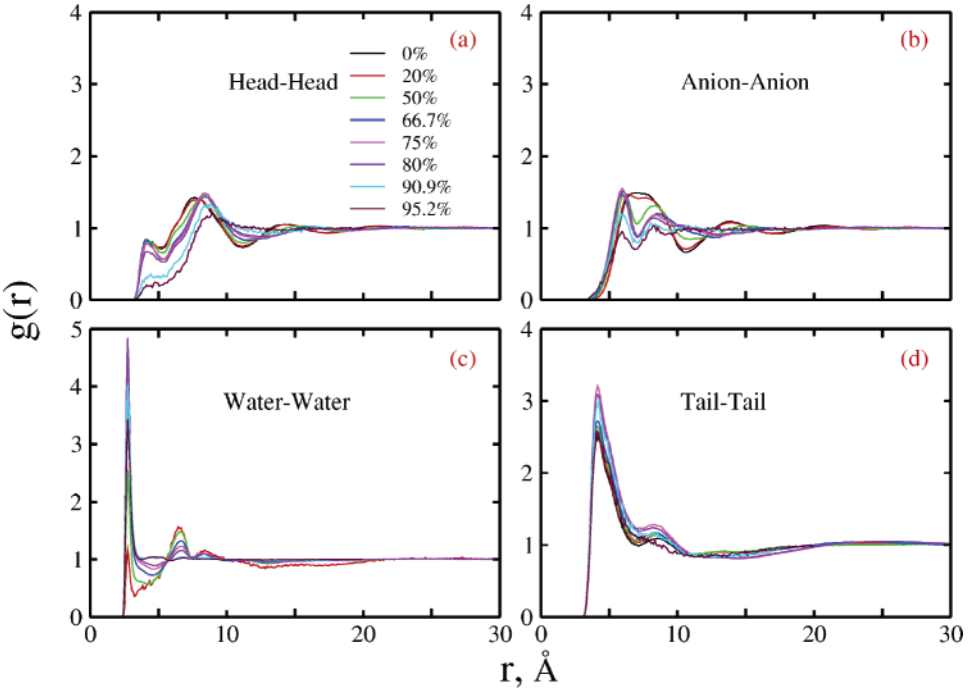

Figure 3. Intermolecular radial distribution functions of center-of-mass for (a) head−head, (b) anion−anion, (c) water−water, and (d) tail−tail.

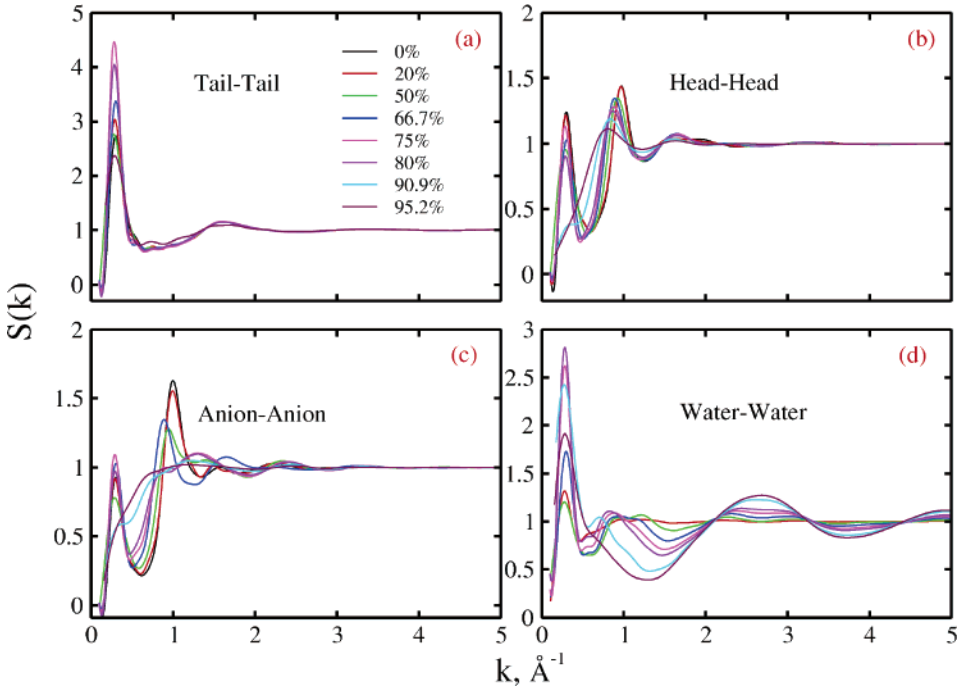

Figure 4. Partial static structure factors for various water concentrations: (a) head−head; (b) anion−anion; (c) water−water and (d) tail−tail. Note that the partial structure factors of tail−tail and water−water have the most conspicuous prepeaks; the prepeaks of head−head and anion−anion almost vanish for water contents of 90.9 and 95.2%.

sluggish increase for less than 50% water content. This trend is in agreement with Hanke and Lynden-Bell's[30] observation for the $DMIM^+/Cl^-$/water mixture. However, the spatial correlations of head−head and anion−anion show a quite different behavior. In panels a and b of Figure 3, it can be seen that the main peaks of head−head and anion−anion RDFs exhibit a "turnover". At a water fraction of 75%, the main peaks become sharpest, indicating the most enhanced spatial correlation. Within the range of water contents studied, the shape of head−head RDFs appears stable until a 90.9% water fraction, despite the displacement of the main peaks due to the intruding water. In contrast, in the anion−anion RDFs, a conspicuous bifurcation of the main peak of dry IL can be found, which demonstrates that the anion−water interaction plays the major role in determining the IL miscibility, in agreement with prevailing concepts.[26,28]

The water structure as affected by the charged polar groups was also investigated. Figure 3c illustrates that the water−water spatial correlation exhibits a significant variation over the range of water fractions, relative to the head−head and anion−anion RDFs. A turnover at an 80% fraction can also be seen. Associated with the fact that the water is embedded in the polar IL network, the strong water−water correlation suggests the formation of a heterogeneous water network.

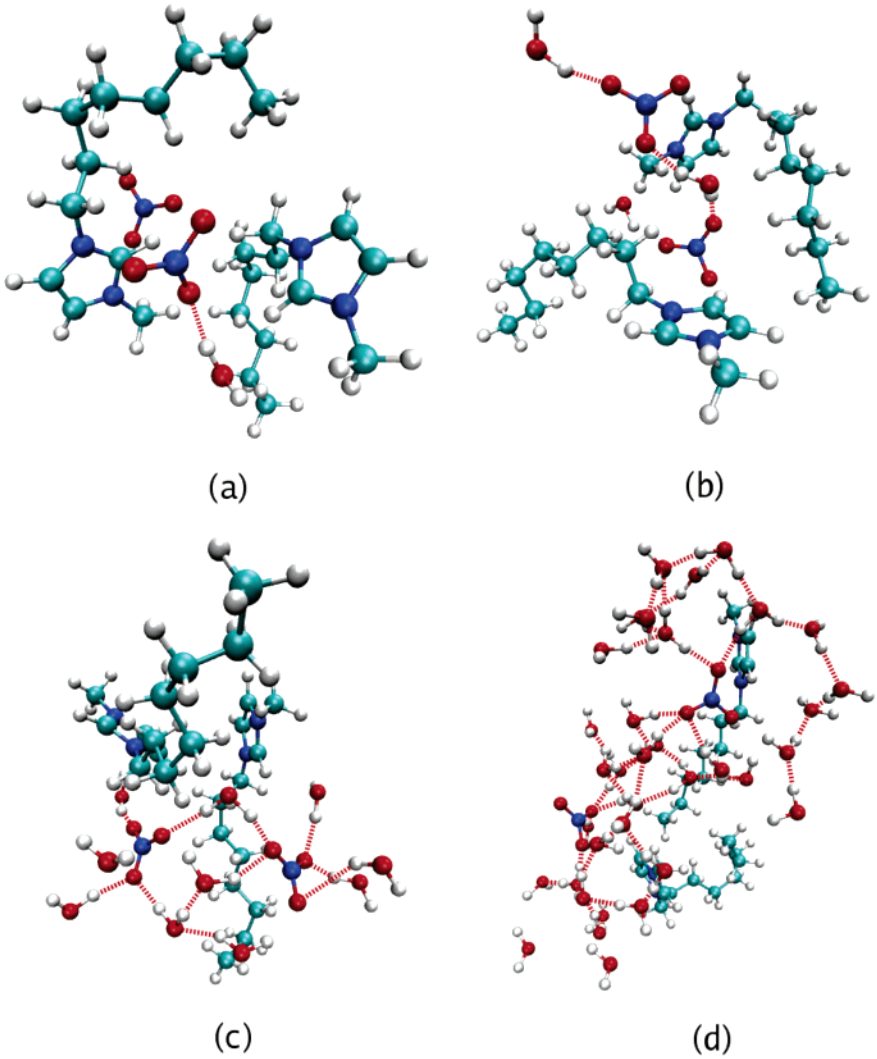

Figure 5. The visualization of anion−water, anion−anion, and water−water interactions. The red dashed line denotes the hydrogen bond. The snapshots correspond to (a) a mixture with water of 20% mole fraction, (b) 50% mole fraction, (c) 80% mole fraction, and (d) 95.2% mole fraction. In each snapshot, the two ion pairs closest to the origin of simulation cell and the water molecules within 6 Å around each of the two selected anions are shown.

It is well-known that surfactant molecules can form micelle structures in aqueous solutions when the concentration of surfactant is greater than the critical micelle concentration (CMC).[34,44−47] For imidazolium based ILs, which are surfactants of a cationic type, a micellelike structure also has been found computationally[13,14] in dry sample. Therefore, the snapshots of Figure 1 provide a picture of the evolution of the micelle structure in response to the changing amount of water. The primary characteristics of this structure are that, in addition to the phase separation between polar and nonpolar groups, there is also a stronger spatial correlation between the terminal tail−tail groups than between the parts of the chain that are closer to the polar headgroup. As such, the terminal tail groups can form prominent aggregation, consistent with our previous observation.[13] In Figure 3d, it can be seen that the tail aggregation has been enhanced by the intruding water, as compared to the dry IL. Furthermore, the main peaks of tail−tail RDFs show an interesting turnover. At water fraction 75%, the main peak appears sharpest and much higher than the polar groups, demonstrating a significantly enhanced tail aggregation.

With the results shown in Figures 1 and 3 in hand, a conclusion is that the most tightly aggregated micelle structure is formed at ∼75−80% water fraction. In panels d and e of Figure 1, it can be seen that blocks of nonpolar groups are confined in a polar network, including small water clusters, resembling a typical wormlike micelle. For the mixtures of mole fraction 90.9 and 95.2%, from the RDFs of Figure 3, it can be seen that the head−head and anion−anion distributions show very weak spatial correlation due to the overriding water fraction, with the ions being highly diffusive, in accordance with the dispersion of polar groups shown in Figure 1f. However, the nonpolar groups remain considerably aggregated, regardless of the collapse of the polar network, indicating the existence of a loose micelle structure. This fact suggests that the range of IL concentrations studied here goes higher than the CMC, after which no micelle can exist. The above result shows the trend of evolution of the micelle structure and agrees with the prediction of a CMC.

C. Intermediate Range Order. To quantitatively investigate the characteristic length scale of the structural organization, the partial static structure factor, S_{ij}, corresponding to the partial RDFs, g_{ij}, was calculated according to eq 2, where ρ is the number density of the centers of mass of interest, and $S_{ij}(k)$ is given by

$$S_{ij}(k) = 1 + \frac{4\pi\rho}{k}\int_0^\infty [g_{ij}(r) - 1]r \sin(rk)\, dr \qquad (2)$$

The minimum k value was set to $2\pi/L$, where the L is the side length of each simulation cell.

The results for the partial structure factors of tail−tail, head−head, anion−anion, and water−water are shown in Figure 4, respectively. In panels a, b, and c, the most striking feature in the structure factors is the coexistence of a main peak, reflecting the spatial correlation between successive neighbor solvation shells, and another sharp prepeak at around 0.3 $Å^{-1}$. This prepeak is a typical "first sharp diffraction peak",[48,49] which indicates the appearance of intermediate range order. Both Urahata and Ribeiro[10] and Lopes and Pádua[14] have reported a similar prepeak in neat (dry) ILs. In panel d, in addition to the prepeak, there are also other structural peaks, which reflect the multiple characteristic length scales of the hydrogen bond network of water, with their positions in good agreement with experiment.[50] It can be seen that the characteristic length scale of the water network is strongly affected by the phase separations. For example, for most water contents studied, the structural peaks of neat water have been quenched due to the appearance of the prepeak, whereas for mole fraction 90.9 or 95.2%, the structure factor of the water−water correlation remains an obvious prepeak, although the other peaks conspicuously demonstrate the multiple characteristic length scales seen in neat water. It should also be noted that within the range of water contents studied, the structures of tail−tail, head−head, anion−anion, and water−water remain approximately invariant, with a characteristic length scale of ∼20 Å. Near a water fraction of 75−80%, the sharp prepeaks indicate that the most ordered nanostructure forms. In their SANS data analysis for the static structure factor, Bowers et al.[34] found that there exists a sharp structural peak at similar water concentrations for $OMIM^+/Cl^-$ aqueous solution. Because of the similar miscibility of $OMIM^+/Cl^-$ and $OMIM^+/NO_3^-$, it can be concluded that both the present simulated characteristic length scale and the extent of nanostructural organization seen as a function of water content are consistent with the experiment observations.

D. Mechanism of Organization. The turnover in evolution of the micelle structure as a function of water content can be explained as the competition between the persistent hydrophobic interaction of the nonpolar groups and the breakup of the cation head group−anion electrostatic network after the introduction of water. Before the turnover point, the partially unscreened (by water) cation head group−anion electrostatic network causes the head groups to retain a stable spatial correlation, which enhances the continuous enhancement of the tail group aggregation. However, due to the limited H-bonding ability of the anions, there is a range of water contents (∼75−80%) in which the three H-bond acceptors of each nitrate are saturated so that the cation head group−anion electrostatic interactions are strongly screened by the water molecule hydrogen bonded to the anions. Thereafter, due to the head group−head group electrostatic repulsions, which are well-balanced by the anions before the turnover, and the weak water-head group interactions, the spatial correlation of head groups attenuates, directly resulting in the weakening of tail group aggregation. For high water proportions, the structural organization is destroyed by more and more water clusters, and the entire system becomes highly diffusive. In this case, a loose micelle structure, with positive charge on the polar "shell" (cation head groups), can be formed.

The turnover of the water−water correlation results from the competition between the water−water and water−anion interactions. To provide a visual insight, four snapshots taken from MD trajectory data are shown in Figure 5. For lower water concentrations, the anion−water H-bond interactions cause the water molecule to be attracted to the anion. In Figure 5a, it can be seen that a water molecule is hydrogen-bonded to an anion, whereas in Figure 5b, two anions and two water molecules form a chainlike structure by three O−H hydrogen bonds. As the water content increases, more and more water molecules gather around anions so that the "passive" water aggregation reaches a limit at which the hydrogen bonding of the anions is "saturated". In Figure 5c, such a saturation process can be seen. On the other side, the water molecule confined between two neighboring nitrates can play the role of an "extra bond", causing the strongest anion−anion correlation. It also should to be stressed that the above associated aggregation of water depends on the strong basicity and planar symmetry of nitrate. Otherwise, only a loose water−anion network or a free-water state would be observed. This finding is in agreement with the observation that liquidlike associated aggregates of water can be formed in ILs with the nitrate anion.[26] After the turnover point, the "active" water−water interactions dominate, causing the water−water correlation to be closer to the neat system. In Figure 5d, it can be seen that in addition to the water molecules hydrogen-bonded to the two nitrates, a more complex water−water hydrogen bond network has formed, decreasing the density of water molecules aggregating around the anions.

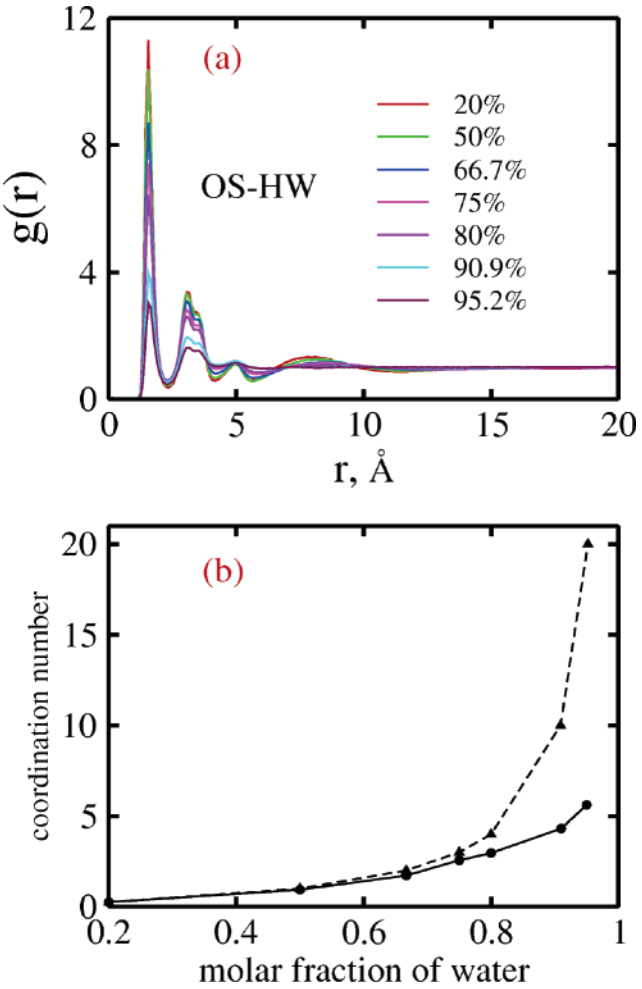

Figure 6. Hydrogen bond interaction between anion and water. (a) Radial distribution functions of the oxygen on the NO_3^- (OS) and the hydrogen on water molecule (HW) in the mixtures. (b) Simulated coordination numbers of water in the first solvation shell of the anions (black solid line), as compared to the corresponding molar ratio of water to IL (dashed line).

Figure 6 provides quantitative support for above analysis. In Figure 6a, the sharp, main peaks of water hydrogen−nitrate oxygen RDFs located at ∼1.5 Å indicate the strong water−anion H-bond interactions; in Figure 6b, it can be seen that with increasing water content, the coordination number of water molecules in the first solvation shell of the anion increases accordingly, and is close to the mole ratio of water molecules to ion pairs up to the fraction 90.9%. It should be noted that at a water fraction of 80%, the coordination number is 2.96, closely related to the three H-bond acceptors of nitrate. For higher water proportions, the increase in coordination number is slower than the increase in the molar ratio of water molecules to ion pairs, demonstrating that the water−water interactions have begun to dominate the water−anion interactions.

IV. Concluding Remarks

The results of the present MD simulations demonstrate that an imidazolium-based, room temperature ionic liquid can be induced to form organized nanostructures by introducing a certain range of water content, relative to the dry sample. The most ordered nanostructure forms when the hydrogen bonding ability of the anions is saturated by the water. This finding can be generalized to other water-miscible ILs. Correlated with this H-bond saturation, a liquidlike aggregation of water is formed, in agreement with experiment.[26] Since the hydrophilicities of ILs are mainly determined by the anions,[26,28] further simulation work is necessary to investigate the role of other anions on the location of turnover point, which might provide potential directions for a "tunable" nanostructural design concept. The finding of water aggregation in the present study implies that other anions of strong basicity and complex geometry, such as $CF_3CO_2^-$, may result in a more intricate behavior with the water content. A study on the effect of different combinations of counterions and cation chain lengths on the characteristic length scale of nanostructural organization and the shape of the resulting aggregates may also be useful. The proposed mechanism for nanostructural organization in IL−water mixtures may prove helpful in understanding how ILs can participate in mixed solvent systems. The present findings may also be applicable to liquid crystal design and in tuning chemical synthesis. The possibilities will be explored in future research.

Acknowledgment. This research was supported by the Air Force Office of Scientific Research. The authors thank Dr. Tianying Yan, Dr. Gary Ayton, and Dr. Satoru Iruchi for valuable discussions. This research was supported in part by the National Science Foundation through Teragrid resources provided by PSC and TACC.

References and Notes

(1) Rogers, R. D.; Seddon, K. R. *Science* **2003**, *302*, 792.
(2) Wasserscheid, P.; Keim, W. *Angew. Chem., Int. Ed.* **2000**, *39*, 3772.
(3) Welton, T. *Chem. Rev.* **1999**, *99*, 2071.
(4) Gordon, C. M.; Holbrey, J. D.; Kennedy, A. R.; Seddon, K. R. *J. Mater. Chem.* **1998**, *8*, 2627.
(5) Hagiwara, R.; Ito, Y. J. *Fluorine Chem.* **2000**, *105*, 221.
(6) Holbrey, J. D.; Seddon, K. R. *J. Chem. Soc., Dalton Trans.* **1999**, 2133.
(7) Lee, K. M.; Lee, C. K.; Lin, I. J. B. *Chem. Commun.* **1997**, 899.
(8) Lee, C. K.; Huang, H. W.; Lin, I. J. B. *Chem. Commun.* **2000**, 1911.
(9) Hamaguchi, H.; Ozawa, R. *Adv. Chem. Phys.* **2005**, *131*, 85.
(10) Urahata, S. M.; Ribeiro, M. C. C. *J. Chem. Phys.* **2004**, *120*, 1855.
(11) Margulis, C. J. *Mol. Phys.* **2004**, *102*, 829.
(12) Wang, Y.; Voth, G. A. *J. Am. Chem. Soc.* **2005**, *127*, 12192.
(13) Wang, Y.; Jiang, W.; Voth, G. A. Spatial Heterogeneity in Ionic Liquids. In *Ionic Liquids Not Just Solvents Anymore*; Brennecke, J. F., Rogers, R. D., Sedden, K. R., Eds.; ACS Symposium Series; American Chemical Society: Washington, DC, 2007; in press.
(14) Canongia Lopes, J. N.; Padua, A. A. H. *J. Phys. Chem. B* **2006**, *110*, 3330.
(15) Bowers, J.; Vergara-Gutierrez, M. C. *Langmuir* **2004**, *20*, 309.
(16) Baldelli, S. J. *J. Phys. Chem. B* **2003**, *107*, 6148.
(17) Lynden-Bell, R. M. *Mol. Phys.* **2003**, *101*, 2625.
(18) Lynden-Bell, R. M.; Del Popolo, M. G. *Phys. Chem. Chem. Phys.* **2006**, *8*, 949.
(19) Lynden-Bell, R. M.; Kohanoff, J.; Del Popolo, M. G. *Faraday Discuss.* **2005**, *129*, 57.
(20) Yan, T.; Li, S.; Jiang, W.; Gao, X.; Xiang, B.; Voth, G. A. *J. Phys. Chem. B* **2006**, *110*, 1800.
(21) Jiang, W.; Wang, Y.; Yan, T.; Voth, G. A. **2006**, in press.
(22) Kazarian, S. G.; Briscoe, B. J.; Welton, T. *Chem. Commun.* **2000**, 2047.
(23) Aki, S. N. V. K.; Brennecke, J.; Samanta, A. *Chem. Commun.* **2001**, 413.
(24) Tran, C. D.; De Paoli, L.; Silvia, H.; Oliveira, D. *Appl. Spectrosc.* **2003**, *57*, 152.
(25) Welton, T.; Wasserscheid, P.; Eds. Wiley-VCH: Weinheim, Germany, 2003.
(26) Cammsrata, L.; Kazarian, S. G.; Salter, P. A.; Welton, T. *Phys. Chem. Chem. Phys.* **2001**, *3*, 5192.
(27) Seddon, K. R.; Annegret., S.; Maria-Jose., T. *Pure. Appl. Chem.* **2000**, *72*, 2275.
(28) Rivera-Ruberto, S.; Baldelli, S. *J. Am. Chem. Soc.* **2004**, *126*, 11788.
(29) Saha, S.; Hamaguchi, H. *J. Phys. Chem. B* **2006**, *110*, 2777.
(30) Hanke, C. G.; Lynden-Bell, R. M. *J. Phys. Chem. B* **2003**, *107*, 10873.
(31) Canongia Lopes, J. N.; Costa Gomes, M. F.; Padua, A. A. H. *J. Phys. Chem. B* **2006**, *110*, 16816.
(32) Schroder, U.; Wadhawan, J. D.; Compton, R. G.; Marken, F.; Suarez, P. A. Z.; Consorti, C. S.; de Souza, R. F.; Dupont, J. *New J. Chem.* **2000**, *24*, 1009.
(33) Dupont, J.; de Souza, R. F..; Suarez, P. A. Z. *Chem. Rev.* **2002**, *102*, 3667.
(34) Bowers, J.; Butts, C. P.; Martin, P. J.; Vergara-Gutierrez, M. C. *Langmuir* **2004**, *20*, 2191.
(35) Firestone, M. A.; Dzielawa, J. A.; Zapol, P.; Curtiss, L. A.; Seifert, S.; Dietz, M. L. *Langmuir* **2002**, *18*, 7258.
(36) Antonietti, M.; Kuang, D.; Smarsly, B.; Zhou, Y. *Angew. Chem., Int. Ed.* **2004**, *43*, 4988.
(37) Malham, I. B.; Letellier, P.; Turmine, M. *J. Phys. Chem. B* **2006**, *110*, 14212.
(38) Cornell, W. D.; Cieplak, P.; Bayly, C. I.; Gould, I. R.; Merz, K. M.; Ferguson, D. M.; Spellmeyer, D. C.; Fox, T.; Caldwell, J. W.; Kollman, P. A. *J. Am. Chem. Soc.* **1995**, *117*, 5179.
(39) Yan, T.; Burnham, C. J.; Del Popolo, M. G.; Voth, G. A. *J. Phys. Chem. B* **2004**, *108*, 11877.
(40) Yan, T.; Burnham, C. J.; Wang, Y. T.; Gao, X. P.; Voth, G. A. to be submitted.
(41) Frisch, M. J.; Trucks, G. W.; Schlegel, H. B.; Scuseria, G. E.; Robb, M. A.; Cheeseman, J. R.; Montgomery, J. J. A.; Vreven, T.; Kudin, K. N.; Burant, J. C.; Millam, J. M.; Iyengar, S. S.; Tomasi, J.; Barone, V.; Mennucci, B.; Cossi, M.; Scalmani, G.; Rega, N.; Peterson, G. A.; Nakatsuji, H.; Hada, M.; Ehara, M.; Toyota, K.; Fukuda, R.; Hasegawa, J.; Ishida, M.; Nakajima, T.; Honda, Y.; Kitao, O.; Nakai, H.; Klene, M.; Li, X.; Knox, J. E.; Hratchian, H. P.; Cross, J. B.; Bakken, V.; Adamo, C.; Jaramillo, J.; Gomperts, R.; Stratmann, R. E.; Yazyev, O.; Austin, A. J.; Cammi, R.; Pomelli, C.; Ochterski, J. W.; Ayala, P. Y.; Morokuma, K.; Voth, G. A.; Salvador, P.; Dannenberg, J. J.; Zakrzewski, V. G.; Dapprich, S.; Daniels, A. D.; Strain, M. C.; Farkas, O.; Malick, D. K.; Rabuck, A. D.; Raghavachari, K.; Foresman, J. B.; Ortiz, J. V.; Cui, Q.; Baboul, A. G.; Clifford, S.; Cioslowski, J.; Stefanov, B. B.; Liu, G.; Liashenko, A.; Piskorz, P.; Komaromi, I.; Martin, R. L.; Fox, D. J.; Keith, T.; Al-Laham, M. A.; Peng, C. Y.; Nanayakkara, A.; Challacombe, M.; Gill, P. M. W.; Johnson, B.; Chen, W.; Wong, M. W.; Gonzalez, C.; Pople, J. A. *Gaussian 03*, Revision C. 02; Gaussian, Inc.: Wallingford CT, 2004.
(42) Wu, Y.; Tepper, H. L.; Voth, G. A. *J. Chem. Phys.* **2006**, *124*, 024503.
(43) DL_POLY User Manual. Forester, T. R. S.; W. CCLRC, D. L.: Daresbury, Warrington, UK. 1995.
(44) Smit, B.; Esselink, K.; Hilbers, P. A. J.; Van Os, N. M.; Rupert, L. A. M.; Szleifer, I. *Langmuir* **1993**, *9*, 9.
(45) Palmer, B. J.; Liu, J. *Langmuir* **1996**, *12*, 746.
(46) Marrink, S. J.; Mark, A. E. *J. Am. Chem. Soc.* **2003**, *125*, 15233.
(47) Consorti, C. S.; Suarez, P. A. Z.; de Souza, R. F.; Burrow, R. A.; Farrar, D. H.; Lough, A. J.; Loh, W.; da Silva, L. H. M.; Dupont, J. *J. Phys. Chem. B* **2005**, *109*, 4341.
(48) Madden, P. A.; Wilson, M. *J. Phys.: Condens. Matter* **2000**, *12*, A95.
(49) Barker, D. R.; Wilson, M.; Madden, P. A. *Phys. Rev. E: Stat. Phys., Plasmas, Fluids, Relat. Interdiscip. Top.* **2000**, *62*, 1427.
(50) Saito, S.; Ohmine, I. *J. Chem. Phys.* **1995**, *102*, 3566.